PROCEEDINGS OF SCIENCE

Nucleon structure with pion mass down to 149 MeV

Jeremy Green[*,a] **Michael Engelhardt,**[b] **Stefan Krieg,**[cd] **John Negele,**[a] **Andrew Pochinsky**[a] **and Sergey Syritsyn**[e]

[a] *Center for Theoretical Physics, Massachusetts Institute of Technology, Cambridge, Massachusetts 02139, USA*
[b] *Department of Physics, New Mexico State University, Las Cruces, New Mexico 88003, USA*
[c] *Bergische Universität Wuppertal, D-42119 Wuppertal, Germany*
[d] *IAS, Jülich Supercomputing Centre, Forschungszentrum Jülich, D-52425 Jülich, Germany*
[e] *Lawrence Berkeley National Laboratory, Berkeley, California 94720, USA*
E-mail: jrgreen@mit.edu, engel@physics.nmsu.edu, s.krieg@fz-juelich.de, negele@mit.edu, avp@mit.edu, ssyritsyn@lbl.gov

We present isovector nucleon observables: the axial, tensor, and scalar charges and the Dirac radius. Using the BMW clover-improved Wilson action and pion masses as low as 149 MeV, we achieve good control over chiral extrapolation to the physical point. Our analysis is done using three different source-sink separations in order to identify excited-state effects, and we make use of the summation method to reduce their size.

The 30th International Symposium on Lattice Field Theory
June 24 – 29, 2012
Cairns, Australia

[*] Speaker.

1. Introduction

Lattice QCD calculations of nucleon structure observables are now entering the stage where they are being seriously confronted with experiment, although resources are not sufficient for full control over all systematic errors. Thus, when predicting unobserved quantities, it is useful to know which sources of systematic error must be more carefully controlled in order to achieve agreement for experimentally observed quantities, and which sources of error are already well under control when using standard techniques.

We report on two experimentally measured observables, the isovector Dirac radius $(r_1^2)^v$ and the axial charge g_A; and two predictions, the tensor and scalar charges, g_T and g_S. Proton matrix elements of the vector current are parameterized by two form factors,

$$\langle p(P')|\bar{q}\gamma^\mu q|p(P)\rangle = \bar{u}(P')\left(\gamma^\mu F_1^q(Q^2) + \tfrac{i\sigma^{\mu\nu}\Delta_\nu}{2m}F_2^q(Q^2)\right)u(P), \tag{1.1}$$

where $\Delta = P' - P$ and $Q^2 = -\Delta^2$. The isovector Dirac radius is defined from the slope of the isovector $F_1^v \equiv F_1^u - F_1^d$ at zero momentum transfer:

$$F_1^v(Q^2) = F_1^v(0)(1 - \tfrac{1}{6}(r_1^2)^v Q^2 + \mathcal{O}(Q^4)). \tag{1.2}$$

In terms of experimental observables, $(r_1^2)^v$ is related to the difference between proton and neutron charge radii, the former of which has a 7σ discrepancy between measurements from electron-proton scattering [1] and a recent result using a precise measurement of the Lamb shift in muonic hydrogen [2]. Lattice QCD calculations with a precision of a few percent could help to resolve this.

The axial, tensor, and scalar charges all have similar definitions from neutron-to-proton transition matrix elements at zero momentum transfer:

$$\langle p|\bar{u}\gamma^\mu\gamma_5 d|n\rangle = g_A\bar{u}_p\gamma^\mu\gamma_5 u_n, \qquad \langle p|\bar{u}\sigma^{\mu\nu}d|n\rangle = g_T\bar{u}_p\sigma^{\mu\nu}u_n, \qquad \langle p|\bar{u}d|n\rangle = g_S\bar{u}_p u_n. \tag{1.3}$$

The axial charge is a key benchmark observable, since it is a naturally isovector quantity (and thus not requiring disconnected diagrams to calculate it), measured via forward matrix elements, and it is also well-measured experimentally via beta decay of polarized neutrons.

The tensor and scalar charges have not been measured experimentally, but it has recently been shown [3] that they control the leading contributions to neutron beta decay from new (beyond the Standard Model) physics, and thus they provide a useful input to the analysis of experimental data.

2. Methodology

The main results presented are from calculations performed on ten Lattice QCD ensembles using $2+1$ flavors of tree-level clover-improved Wilson fermions coupled to double HEX-smeared gauge fields [4]. We also compare with results from earlier $2+1$ flavor calculations [5, 6, 7] using four ensembles with unitary domain wall fermions [8, 9], as well as five ensembles using a mixed-action scheme with domain wall valence quarks and Asqtad staggered sea quarks [10]. The ranges of parameters used in these calculations are summarized in Tab. 1 and Fig. 1.

On every ensemble with Wilson fermions, we compute nucleon three-point functions using three different source-sink separations T. When matrix elements are computed using the traditional ratio-plateau method, the asymptotically dominant excited-state contaminations arise from transitions

Action	a (fm)	m_π (MeV)	L_x/a	L_t/a	T/a	# meas
Wilson	0.09	317(2)	32	64	10, 13, 16	824
Wilson	0.116	149–356	24, 32, 48	24, 48, 96	8, 10, 12	762–10032
Domain wall	0.084	297–403	32	64	12	4216–7056
Domain wall	0.114	329(5)	24	64	9	3192
Mixed	0.124	293–597	20, 28	64	9	2176–5024

Table 1: Lattice actions and ranges of parameters used: lattice spacing, pion mass, spatial and temporal box size, source-sink separation, and number of measurements.

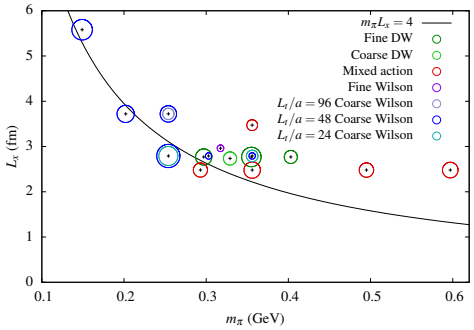

Figure 1: Spatial box length L_x and pion mass for the full set of ensembles. The areas of the circles are proportional to the number of measurements made on each ensemble.

between the ground state and the lowest excited state, and these decay as $e^{-\Delta E T/2}$. The summation method requires combining more than one source-sink separation, but yields improved asymptotic behavior, with the leading contaminants to forward matrix elements decaying as $Te^{-\Delta E T}$ [11, 12].

This set of ensembles allows for control over, or study of, various sources of systematic error. In roughly decreasing order of the level of control that we can achieve:

Quark masses For all ensembles, the strange quark mass is near the physical value. Our smallest m_{ud} corresponds to a pion mass of 149 MeV, which is just 10% above the physical pion mass. This allows for either a direct comparison of the $m_\pi = 149$ MeV ensemble with experiment, or a comparison after a mild chiral extrapolation to the physical pion mass.

Excited states Using the ratio-plateau method with three different source-sink separations allows for clear identification of observables where excited-state contamination is a problem. These three source-sink separations can also be combined using the summation method to get another result that may be less affected by excited states.

Finite volume In general, finite-volume effects are expected to be small with $m_\pi L \gtrsim 4$. Furthermore, we can perform controlled comparisons between the $24^3 \times 48$ and $32^3 \times 48$ Wilson ensembles near $m_\pi = 250$ MeV, where the spatial volume is changed while other parameters are fixed.

Finite temperature At our smallest pion masses, the lattice time extent is shorter than the typically used $L_t = 2L_x$, and these ensembles may be particularly susceptible to thermal effects. On the other hand, the three different time extents $L_t/a \in \{24, 48, 96\}$ used for Wilson ensembles near $m_\pi = 250$ MeV are useful for identifying possible problems.

Discretization The use of different lattice actions and different lattice spacings allows for a consistency check, but this set of ensembles is insufficient for taking a continuum limit.

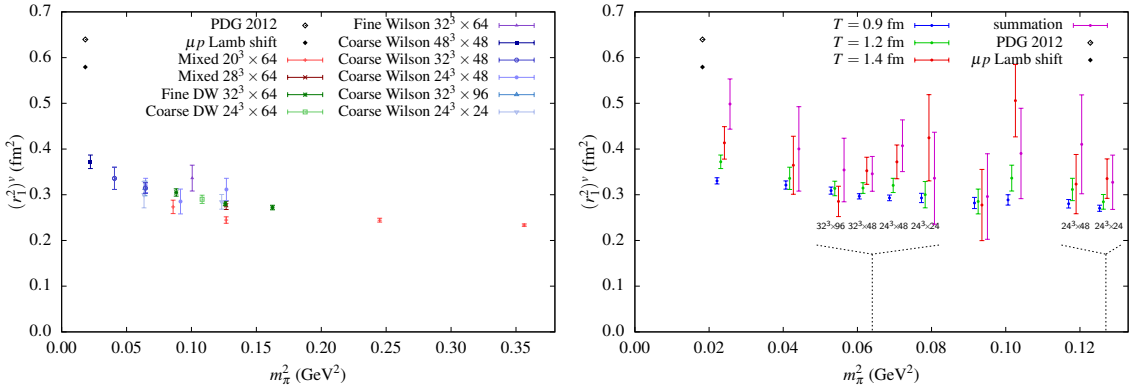

Figure 2: Isovector Dirac radius $(r_1^2)^v$, as determined from dipole fits to $F_1(Q^2)$. The two experimental points both use the PDG [1] value for $(r_E^2)^n$, and $(r_E^2)^p$ is taken from either the PDG or from the result from measurement of the Lamb shift in muonic hydrogen [2]. **Left:** Results from ensembles using the three different lattice actions. Wilson action points are taken from the middle source-sink separation. **Right:** The full set of Wilson action results. Measurements using the three source-sink separations and the summation method are slightly displaced horizontally. The points corresponding to the smallest source-sink separation are placed at the measured value of m_π^2, except for the ensembles with $m_\pi \approx 250$ MeV and $m_\pi \approx 350$ MeV, where the different volumes are displaced horizontally and the dotted lines indicate the approximate measured values of m_π^2.

3. Results

For each of the observables, two plots are shown. The first includes the data from all three actions. In order to show results using similar techniques, the middle source-sink separation on the Wilson action enembles is shown for this comparison. The second plot shows the dependence on source-sink separation and the summation result for each of the ten Wilson ensembles.

Figure 2 shows the isovector Dirac radius. This is extracted from measurements of the isovector Dirac form factor $F_1^v(Q^2)$ via dipole fits $F_1^v(Q^2) \sim \frac{F_1^v(0)}{(1+Q^2/M_D^2)^2}$. The first plot shows a broad consistency among the three lattice actions in their region of overlapping pion masses, although the unitary domain wall data are systematically a bit higher than the mixed action data. There is a gentle rise as m_π approaches the physical value, but all of these data significantly undershoot the experimental results. The second plot shows that excited-state effects are responsible for a large part of this discrepancy with experiment. There is a general trend for the data on each ensemble to increase with source-sink separation, and on the lightest ensemble the summation point is near the experimental points. Chiral extrapolation of the summation data to the physical pion mass yields a result consistent with experiment [13]. As shown in Ref. [13], calculations of the isovector Pauli radius, magnetic moment, and quark momentum fraction behave similarly: results for the 149 MeV ensemble monotonically approach the experimental value with increasing source-sink separation, the summation point agrees with experiment, and a chiral extrapolation of the summation data to the physical pion mass yields results in agreement with experiment and having a smaller statistical uncertainty than the 149 MeV summation point. Further study will be needed to obtain full control over excited-state effects, but with presently available data we consider the summation method as our best approach for reducing their size, and it succeeds in producing agreement with experiment

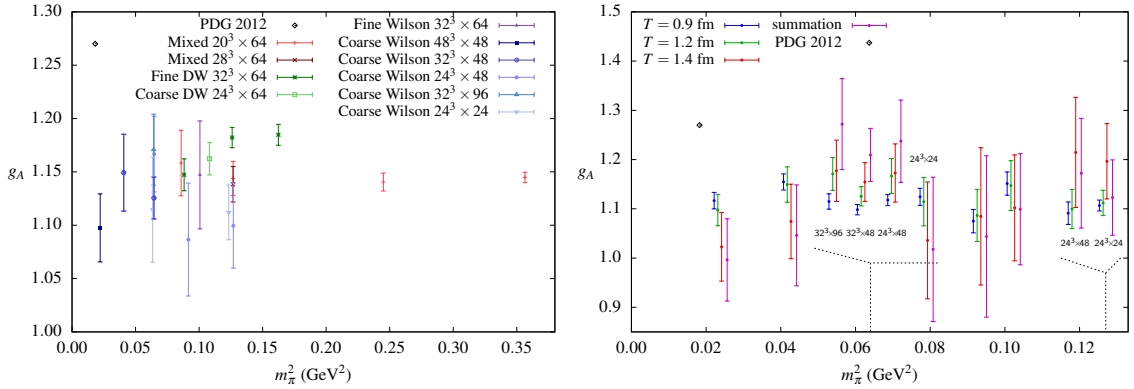

Figure 3: Axial charge g_A. The experimental value is from Ref. [1]. See caption of Fig. 2.

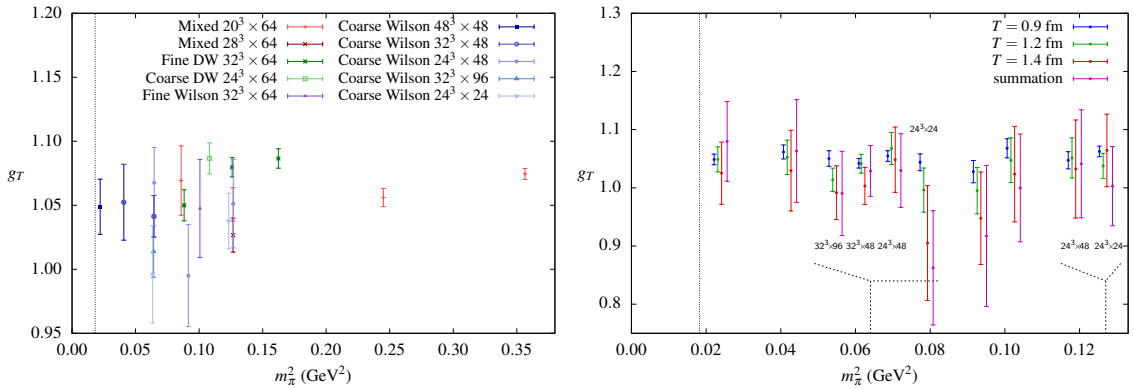

Figure 4: Tensor charge g_T. The physical pion mass is indicated by the vertical line. See caption of Fig. 2.

for these four observables. Comparing the summation data on the four different space-time volumes at $m_\pi \approx 250$ MeV, we see that there is no statistically significant dependence on spatial volume or time extent. The summation point on the fine ensemble at $m_\pi = 317$ MeV is also consistent with those on the nearby coarse ensembles, indicating the absence of discretization effects at this level of precision.

The axial charge g_A is shown in Fig. 3. Again there is broad agreement among the different actions. There is no clear dependence on m_π, and (using the middle source-sink separation for the Wilson ensembles) the data undershoot experiment by about 10%. Looking at the second plot, we see that, on the lightest two ensembles, increasing the source-sink separation moves the data away from experiment. The opposite behavior is seen in a subset of the four $m_\pi \approx 250$ MeV ensembles. For the three with $L_t/a \geq 48$, increasing the source-sink separation moves the data toward experiment and the summation points are consistent with experiment. In contrast, the fourth with $L_t/a = 24$ behaves similarly to the lightest two ensembles, albeit with larger statistical uncertainty. This suggests that the decrease of g_A with source-sink separation is caused by the influence of thermal pion states, since the three ensembles that show this behavior all have small $m_\pi L_t$.

Figures 4 and 5 show the tensor charge g_T and the scalar charge g_S, respectively. Measurements of the latter are much noisier; note the significantly larger range of the vertical axis in Fig. 5

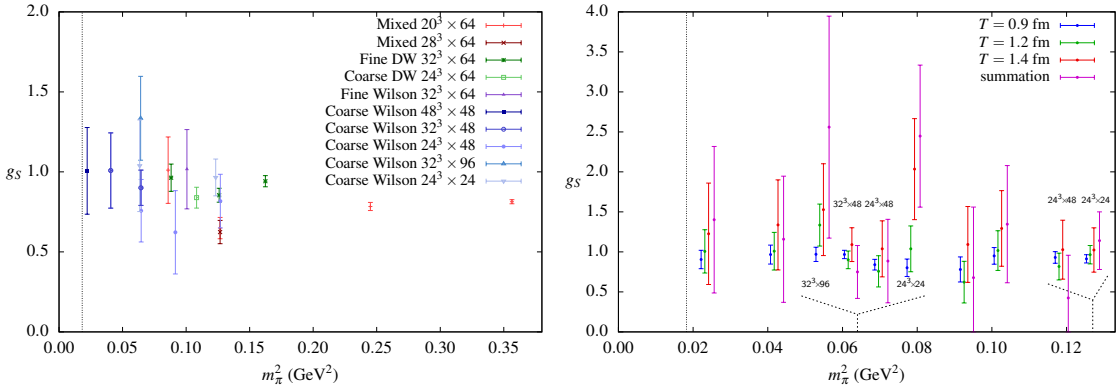

Figure 5: Scalar charge g_S. The physical pion mass is indicated by the vertical line. See caption of Fig. 2.

compared with Figs. 3 and 4. Neither g_S nor g_T shows a clear statistically significant dependence on source-sink separation, so using the middle source-sink separation should give better results than was the case for $(r_1^2)^v$ and g_A. At $m_\pi \approx 250$ MeV, there isn't a significant dependence on the spatial volume, but the ensemble with small L_t shows a dependence on source-sink separation for both g_S and g_T. This behavior isn't seen on the ensembles with the smallest pion masses, so it is likely that they aren't strongly affected by thermal states. From the middle source-sink separation on the $m_\pi = 149$ MeV ensemble, we get $g_S = 1.01(27)$ and $g_T = 1.049(23)$. Extrapolation to the physical pion mass using either the coarse Wilson ensembles, or a global fit to all ensembles, yields results consistent with the lightest ensemble [14].

4. Conclusions

The importance of near-physical quark masses for nucelon structure calculations is illustrated by the isovector Dirac radius, where the rise toward experiment is only seen at our lightest pion masses, and for the axial charge, where new behavior was seen only below $m_\pi \approx 250$ MeV. In addition, it is essential that excited-state effects can be identified, as shown clearly for the isovector Dirac radius. This shows up even more dramatically for the isovector quark momentum fraction $\langle x \rangle_{u-d}$ [15, 13]. More study of excited-state effects is required, and this may require large computing resources, since as the source-sink separation T is increased to reduce excited-state contamination, the signal-to-noise ratio is expected to decay as $e^{-(m_N - \frac{3}{2}m_\pi)T}$ [16]. We have identified finite-temperature effects as a possible source of the discrepancy with experiment for the axial charge.

As we obtain a better understanding of systematic errors, predictions of nucleon properties using Lattice QCD become more credible. Calculations of the nucleon scalar and tensor charge will provide useful input to searches for new physics.

Acknowledgments

We thank Zoltan Fodor for useful discussions and the Budapest-Marseille-Wuppertal collaboration for making some of their configurations available to us. This research used resources of the Argonne Leadership Computing Facility at Argonne National Laboratory, which is supported by

the Office of Science of the U.S. Department of Energy under contract #DE–AC02–06CH11357, resources provided by the New Mexico Computing Applications Center (NMCAC) on Encanto, resources at Forschungszentrum Jülich, and facilities of the USQCD Collaboration, which are funded by the Office of Science of the U.S. Department of Energy.

During this research JG, SK, JN, AP, and SS were supported in part by the U.S. Department of Energy Office of Nuclear Physics under grant #DE–FG02–94ER40818, ME was supported in part by DOE grant #DE–FG02–96ER40965, SS was supported in part by DOE contract #DE–AC02–05CH11231, and SK was supported in part by Deutsche Forschungsgemeinschaft through grant SFB–TRR 55.

The Chroma software suite [17] was used for the mixed action and unitary domain wall calculations. The Wilson-clover calculations were performed with Qlua [18].

References

[1] **Particle Data Group** Collaboration, J. Beringer *et. al.*, *Phys.Rev.* **D86** (2012) 010001.

[2] R. Pohl, A. Antognini, F. Nez, F. D. Amaro, F. Biraben *et. al.*, *Nature* **466** (2010) 213–216.

[3] T. Bhattacharya, V. Cirigliano, S. D. Cohen, A. Filipuzzi, M. Gonzalez-Alonso *et. al.*, *Phys.Rev.* **D85** (2012) 054512 [1110.6448].

[4] S. Dürr, Z. Fodor, C. Hoelbling, S. D. Katz, S. Krieg *et. al.*, *JHEP* **1108** (2011) 148 [1011.2711].

[5] S. N. Syritsyn, J. D. Bratt, M. F. Lin, H. B. Meyer, J. W. Negele *et. al.*, *Phys.Rev.* **D81** (2010) 034507 [0907.4194].

[6] J. D. Bratt *et. al.*, *Phys.Rev.* **D82** (2010) 094502 [1001.3620].

[7] S. Syritsyn, *Exploration of nucleon structure in lattice QCD with chiral quarks*. PhD thesis, MIT, 2010.

[8] **RBC-UKQCD** Collaboration, C. Allton *et. al.*, *Phys.Rev.* **D78** (2008) 114509 [0804.0473].

[9] **RBC-UKQCD** Collaboration, Y. Aoki *et. al.*, *Phys.Rev.* **D83** (2011) 074508 [1011.0892].

[10] C. W. Bernard, T. Burch, K. Orginos, D. Toussaint, T. A. DeGrand *et. al.*, *Phys.Rev.* **D64** (2001) 054506 [hep-lat/0104002].

[11] S. Capitani, B. Knippschild, M. Della Morte and H. Wittig, *PoS* **LATTICE2010** (2010) 147 [1011.1358].

[12] **ALPHA** Collaboration, J. Bulava, M. A. Donnellan and R. Sommer, *PoS* **LATTICE2010** (2010) 303 [1011.4393].

[13] J. R. Green, M. Engelhardt, S. Krieg, J. W. Negele, A. V. Pochinsky *et. al.*, 1209.1687.

[14] J. R. Green, J. W. Negele, A. V. Pochinsky, S. N. Syritsyn, M. Engelhardt *et. al.*, 1206.4527.

[15] J. Green, S. Krieg, J. Negele, A. Pochinsky and S. Syritsyn, *PoS* **LATTICE2011** (2011) 157 [1111.0255].

[16] G. P. Lepage, in *From Actions to Answers: Proceedings of the 1989 Theoretical Advanced Study Institute in Elementary Particle Physics, 5-30 June 1989, University of Colorado, Boulder* (T. DeGrand and D. Toussaint, eds.), pp. 97–120, 1989.

[17] **SciDAC, LHPC, and UKQCD** Collaborations, R. G. Edwards and B. Joó, *Nucl.Phys.Proc.Suppl.* **140** (2005) 832 [hep-lat/0409003].

[18] A. Pochinsky, "Qlua." https://usqcd.lns.mit.edu/w/index.php/QLUA.